Indonesian Journal of Electrical Engineering and Computer Science
Vol. 41, No. 3, March 2026, pp. 885~893
ISSN: 2502-4752, DOI: 10.11591/ijeecs.v41.i3.pp885-893

Intelligent artificial neural network-based control for solar electric vehicle charger

Rajeshkumar Damodharan, Pradeep Kumar S
Department of Electrical and Electronics Engineering, Vels Institute of Science, Technology, and Advanced Studies, Chennai, India

Article Info

Article history:

Received Dec 5, 2025
Revised Jan 11, 2026
Accepted Jan 17, 2026

Keywords:

Artificial neural networks
Electrical vehicle
Maximum power point tracking
Photovoltaic system
Resonant converter

ABSTRACT

The performance of electric vehicle (EV) charging systems in response to sudden changes in solar irradiation and dynamic battery load variations. EV chargers must have effective power conversion and flexibility as the use of renewable energy sources increases. This paper suggests a charging system based on resonant converters that minimizes heat and losses in EV charging stations by enabling high-efficiency, soft-switching power transfer. For modern EV applications, the ability to manage large voltage fluctuations ensures reliable, quick, and portable charging. The artificial neural networks (ANN) controller overcomes the drawbacks of conventional Perturb and Observe (P&O) for solar DC-DC converters and PI control for resonant converter approaches. MATLAB simulation results demonstrate that the proposed system outperforms traditional techniques in terms of an ANN-based controller, which enhances maximum power point tracking (MPPT) efficiency to 98.6%, reduces oscillations near the maximum power point by approximately 80%, and increases total EV charging efficiency by 3%. The ANN-based control to EV charging infrastructure greatly enhances overall system dependability and real-time responsiveness, making it a good fit for subsequent smart grid and renewable energy applications.

Corresponding Author:

Rajeshkumar Damodharan
Department of Electrical and Electronics Engineering
Vels Institute of Science, Technology, and Advanced Studies
Pallavaram, Chennai, Tamil Nadu, India-600117
Email: d.rajeshkumar.reddy@gmail.com

1. INTRODUCTION

The renewable energy sources, especially solar power, have become popular in the energy industry and are currently considered environmentally friendly and sustainable. Electric vehicle (EV) charging stations that use solar power do not need to be connected to the utility grid; they just need photovoltaic energy to power electric vehicles with clean energy. These stations offer a fully renewable and self-sufficient charging system, built entirely on solar energy only, which comes in particularly convenient in remote areas or in areas with limited grid coverage [1]-[4]. This fact is that they are not dependent on the traditional sources of power, thus reducing the electricity costs, reducing the risk of grid-related disturbances, and ensuring that they will have reliability in delivering the charges under different sun rays. This completely solar-powered system supports the goals of green mobility as energy is zero-emission in the course of the charging process.

Solar-powered EV charging stations (Figure 1), as shown in Figure 1(a), consist of traditional perturb and observe (P&O) maximum power point tracking (MPPT) and proportional integral (PI) controlled resonant converters, which continue to be commonly used in EV chargers. In addition, the overall control process is illustrated in Figure 1(b) as a flow chart, which depicts the sequence of operations from solar input

through MPPT regulation to resonant converter control. Most of the existing literature considers artificial neural network (ANN)-based MPPT (Stage 1) or advanced converter control independently. Not enough research has been done on the coordinated usage of ANN-based MPPT in Stage 1 and an ANN-controlled resonant converter in Stage 2 under dynamic EV battery conditions and rapid irradiance variation. In order to improve overall efficiency, stability, and transient performance in solar EV charging systems [5], there is an obvious gap in the validation of dual-stage ANN control.

The key contributions of the research work are: i) the development of a dual ANN-based control method for EV charging applications; ii) the 98.6% MPPT efficiency, 96.5% charging efficiency, and a reduction in MPP oscillations by 80% compared to PI and P&O methods; iii) improvement of the stability of the resonant converter, whose gain margin is at 12.4 dB, and phase margin is 62° in various EV load and irradiance conditions; iv) it has much better dynamic stability and the oscillations in the voltage are less than l% near MPP and short settling times in response to changes in load and irradiance.

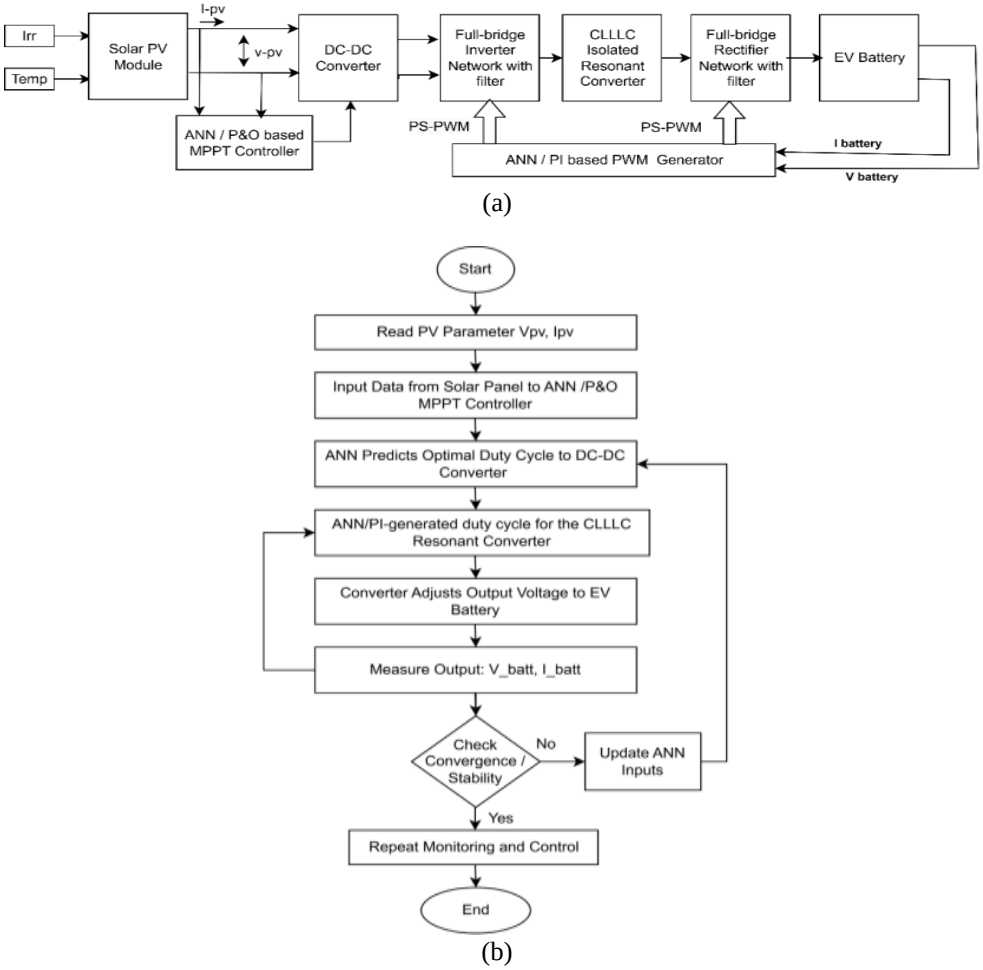

Figure 1. EV charging system: (a) solar MPPT and resonant converter and (b) flow chart

2. MATHEMATICAL MODELLING

2.1. Intelligent solar power optimization

The basic design of a feed-forward ANN output results from Figure 2, where x indicates the ANN input, y represents the output, and w denotes weights and biases. Sigmoidal activation functions power the hidden layers' neurons, along with linear activation in the input and output layers' neurons.

$$y^1 = w2_{10} + w2_{11}.z_1 + w2_{12}z_2 + \cdots + w2_{1n}z_n \quad (1)$$

Therefore, the generalized output equation can be expressed as:

$$y^1 = \sum_{j=0}^{n} w2_{1j} z_j \quad (2)$$

where, $z_0 = 1$ $z_j = f(a_j) = \frac{1}{1+e^{aj}}$ $a_j = \sum_{h=1}^{2} w1_{jh}.x^h$

$$E_{mse} = \frac{1}{n}\sum_{i=1}^{N}(t_i - y_i{}^1)^2 \quad (3)$$

The equation defines the feed-forward (Figure 2(a)) prediction method through N training models, target value ti, and output signal yi at sample i.

Figure 2(b) regression plot shows that two other ANN controllers are developed and trained under supervised learning, which are the solar MPPT and the CLLLC (C: capacitor, L: inductor) resonant converter [6]. ANN-based MPPT uses 2 neurons (PV voltage V_{pv} and current I_{pv} to provide the input layer, and 2 neurons (EV battery voltage V_{bat} and current I_{bat}) to control the resonant converters by the addition of converter output voltage (V_o). To effectively model system non-linearities, both ANNs have 1 hidden layer with 10 neurons and a sigmoid activation function [7]. The optimum switching frequency to the resonant converter and optimum duty ratio to MPPT are given by one neuron in the output layer with a linear activation function. To reduce the mean squared error (MSE) between the reference control signal and the predicted signal, the networks are trained by the backpropagation method with Levenberg-Marquardt optimization, a learning rate of 0.01, and 1000 maximum epochs. By epoch 1000, the gradient became 0.0064034, which indicated that the error surface had converged, whereas the ANN training state. Figure 2(c) illustrates effective and constant learning. The low μ = $1\times10^{-5}$and zero validation checks at epoch 1000 show that smooth optimization without overfitting and high generalization are achieved.

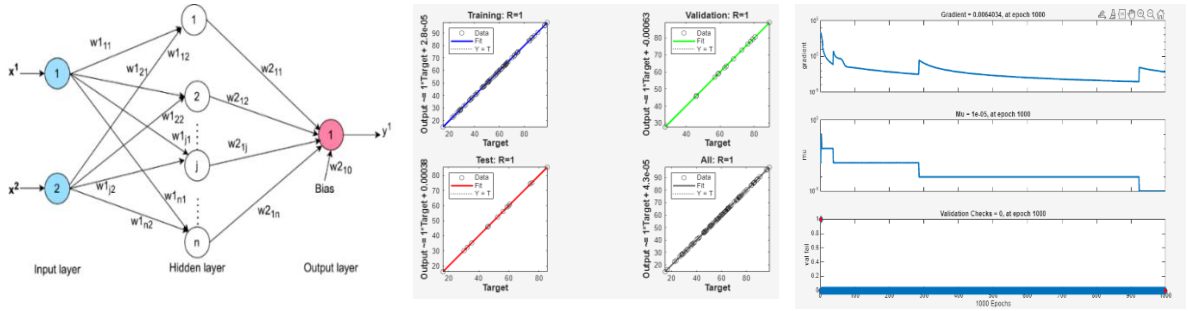

(a) (b) (c)

Figure 2. ANN training: (a) structure of feed-forward neurons, (b) regression plot, and (c) training state plot

2.2. Resonant converter parameter design

The most compelling resonant mode that controls the flow of energy within the CLLLC resonant network is based on the equivalent inductance L_{eq} and the equivalent capacitance C. The quality factor Q is the measure of system efficiency, and Re represents the damping due to the load.

Proper damping as regards load.

$$R_e = \frac{8}{\pi^2} R_L \quad (4)$$

Angular frequency of the resonant wave.

$$\omega_0 = \frac{1}{\sqrt{L_{eq}C}} \quad (5)$$

The series R-L-C resonant subsystem has a quality factor.

$$Q = \frac{1}{R_e}\sqrt{\frac{L_{eq}}{C}} = \frac{\omega_0 L_{eq}}{R_e} = \frac{1}{\omega_0 R_e C} \quad (6)$$

Select the strongest resonant mode in a multi-component CLLLC network to identify an effective $L_{eq}C$, which controls the flow of energy, all of the small signal system onto the strongest resonant mode, and approximate the closed loop transfer between the control action and the appropriate output using a second order form.

$$G_{res}(s) = K \frac{{\omega_0}^2}{s^2+\frac{\omega_0}{Q}S+{\omega_0}^2} \quad (7)$$

Where ω_0 is the natural frequency, and K is the frequency (near resonance) gain. The common denominator coefficients of the second order are:

$$s^2 + 2\zeta\omega_0 s + {\omega_0}^2 \text{ With } \zeta = \frac{1}{2Q} \quad (8)$$

Because it links physical L, C, and R to classical damping ζ and Q, this form is significant [8]-[11].

2.3. ANN-based closed-loop linearized model

The modelling of a small signal converter:

$$\frac{d}{dt}\hat{x} = A\,\hat{x} + B_\omega \hat{\omega}_n + B_{vg}\hat{v}_g + B_d\hat{d}\,,\ \hat{y} = C\,\hat{x} \quad (9)$$

ANN mapping (operating point linearized):

$$\hat{d} = K_{ANN}\hat{Z}, \hat{Z} = H_Z\hat{x}, \quad \hat{d} = K_{ANN}H_Z\hat{x} \quad (10)$$

applying Jacobian (analytic form with a single hidden layer),

$$K_{ANN} = w^{(2)T}D_f W^{(1)} \quad (1 \text{ x m}), \quad (11)$$

where $D_f = diag(z \odot (1-z))$
Substitute (9) into (10),

$$\frac{d}{dt}\hat{x} = (A + B_d\,K_{ANN}H_Z)\hat{x} + B_\omega\hat{\omega}_n + B_{vg}\hat{v}_g \quad (12)$$

State matrix for closed loops,

$$A_{CL} = A + B_d\,K_{ANN}H_Z \quad (13)$$

2.4. ANN's impact on the Q model and model damping

The reduction to the predominant resonant pair (select the resonant eigenmode along the 2×2 modal subspace). Suppose that the lower state vector $\zeta = [\zeta_1, \zeta_2]^T$. The shortened closed-loop linear dynamics are the following:

$$\dot{\zeta} = A_r\zeta + B_r\,\hat{u}_{ext} \quad (14)$$

using a simplified closed-loop matrix:

$$A_{r,CL} = A_r + B_{r,d}\,K_{ANN}H_{Z,r} \quad (15)$$

consider the characteristic polynomial of $A_{r,CL}$, be:

$$\chi(s)=s^2+a_1 s+a_0 \quad (16)$$

then identity:

$$\omega_{0,cl} = \sqrt{a_0},\ \zeta_{cl} = \frac{a_1}{2\sqrt{a_0}},\ Q_{cl} = \frac{1}{2\zeta_{cl}} = \frac{\sqrt{a_0}}{a_1} \quad (17)$$

The K_{ANN} influences the coefficients a_1 and a_0. In particular, the effective stiffness ${\omega_0}^2$ is connected with a_0. There is a direct correlation between a_1 and damping ($\propto \omega_0/Q$). A damping increase or decrease (i.e., lowering or raising Q) will be observed when the ANN adds an effective negative or positive feedback, which alters a_1.

2.5. Eigenvalue testing and stability criterion

Eigenvalue test (sufficient and required for linearized models). Compute eigenvalues λ_i of A_{CL}. Stable (local): $\Re\lambda_i < 0$ for all i. Lyapunov LMI (sufficient), find $P = P^T > 0$ that satisfies the linear matrix inequality (LMI):

$$A_{CL}^T P + P A_{CL} < 0 \tag{18}$$

Assuming this is possible, the linearized closed loop is exponentially stable, and $V = \xi^T P\, \xi$ is a Lyapunov function. Loop margin (gain & phase) frequency domain [12], whereby we linearize the ANN as a gain $K_{ANN} H_Z$ in the d path, and transfer loop L(s) in the ANN output back to the ANN input (where the ANN measures error). In the case of ANN, say that the output error is then:

$$L(s) = G_{ed}(s)\, K_{ANN} \tag{19}$$

The gain margin (GM) and phase margin (PM) from Nyquist/Bode of L(s). Typical design requirements include PM ≥ 30° and GM ≥ 6 dB for robustness.

3. RESULTS AND DISCUSSION

The results reveal that the solar PV system that is regulated by the MPPT converter produces a stable 400 V DC to run the power stage (Figure 3). This DC input is then converted into a CLLLC resonant converter, where the DC is converted to AC by the primary converter and converted to DC again by the secondary converter through a high-frequency 100 kHz transformer. The converter is a highly efficient, low-ripple, smooth dynamic response load and radiation changes on the 360 V, 82 Ah lithium-ion EV battery [13]-[16].

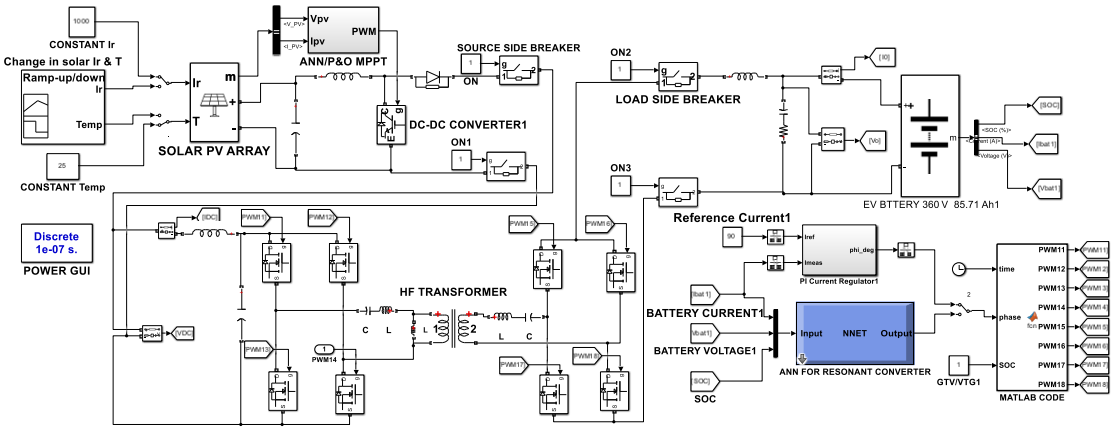

Figure 3. Solar energy EV charging system

3.1. Dynamic behaviour of the solar system and EV battery load

The solar system performance under varying solar conditions, the conventional controller offers slow performance while producing power and voltage oscillations during specific periods of 0.4s to 0.6s, resulting in deteriorated system functions as solar radiation changes by 600 W/m^2, and MPPT voltage and power are reduced to 300 V and 30 KW (Figure 4). The ANN system functions through rapid control systems to maintain a dependable, stable, optimal voltage of 350 V and 40 KW as shown in Figures 4(a) and 4(b). ANN-based MPPT shows fast adaptation at 600, 800, and 900 W/m^2 through which it achieves consistent and efficient power tracking performance. Figure 4(c) makes it evident how well the ANN-based controller reacts to dynamic variations in the load current of the EV battery.

First, the EV battery load is kept at 50 A between 0 and 0.05 seconds, which indicates a low-demand situation. In order to supply the necessary current, the controller modifies the duty cycle when the load rises to 65 A between 0.05 and 0.15 seconds. The dynamically adjusted ANN-based controller to adjust the duty cycle to sustain the performance of the charge-up is stable as the load increases further, up to 0.3 seconds, and limitingly reaches 80 A. Between 0.3 and 0.4 seconds, the load drops to 75 A, and this triggers the controller to adjust the duty cycle and ensure a smooth and efficient EV charging process. ANN-based

controller ensures a constant current charging of batteries without creating sudden variations by automatically adapting to the changing load demands of all these times [17]-[20]. In the PI controller Figure 4(d), it is possible to observe oscillations at the beginning of every load transition, unlike the smooth converter control and adaptive response in the ANN-based controller.

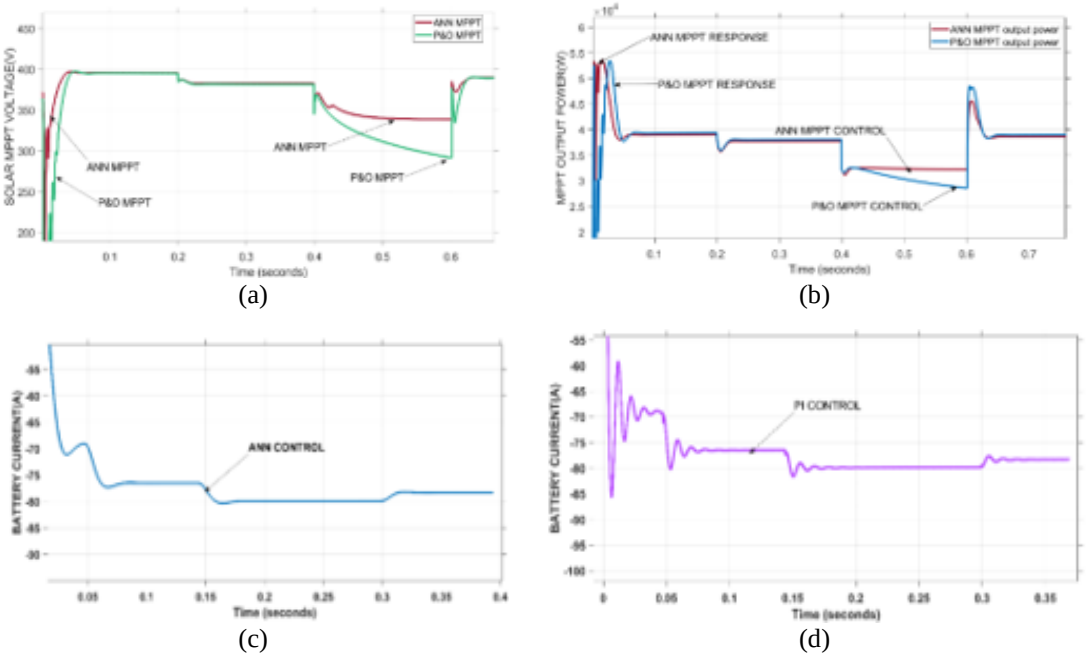

Figure 4. Fluctuation of source and EV load; (a) solar voltage (b) solar power (c) ANN control EV battery current, and (d) PI control battery current

3.2. Comparative performance of dual-stage ANN-based and conventional control techniques

Comparative analysis performance is shown in Figure 5. In Stage 1, as shown in Figure 5(a), ANN-based MPPT was superior to the traditional P&O method because it had achieved a lower steady-state oscillation near the maximum power point of 15% to 2%, reduced tracking time of 90 ms compared to 250 ms, and better tracking performance of 94.2% versus 99.2% with different irradiance conditions. Stage 2, as shown in Figure 5(b), the ANN-controlled CLLLC resonant converter was better than PI control in stability and regulation, the THD decreased to 4.3%, settling time reduced to 65 ms compared to 180 ms, and the output voltage deviation dropped to ±1.2% as compared to PI control of ±4%. Moreover, converter efficiency increased to 96.5%, which proves that the proposed ANN-based dual control system significantly enhances the quality of power, the dynamic response, and the charging efficiency of solar EV charging systems [21]. The proposed ANN-based controller and the traditional PI-controlled system achieved improvement compared in Table 1

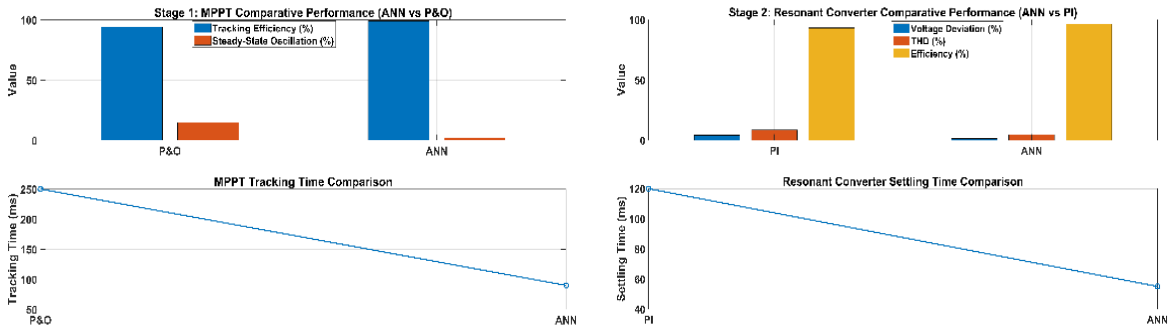

Figure 5. Comparative analysis; (a) ANN Vs P&O MPPT and (b) ANN Vs PI control resonant converter

Table 1. The performance of solar MPPT using P&O and ANN control methods

Performance metric	Conventional PI-controlled system	Proposed ANN-based controlled system	Improvement achieved
Efficiency of MPPT tracking (%)	94.2%	98.6%	+4.4%
Total efficiency of the charger (%)	95.0%	96.5%	+1.5%
Voltage ripple (%) in DC output	4.8%	1.6%	66.7% reduction
Error in steady-state voltage (V)	±8 V	±2 V	75% reduction
Overshoot while changing the load (%)	9.5%	2.3%	75.8% reduction
Irradiance change response time (ms)	150 ms	55 ms	63.3% faster
Power oscillation with changes in irradiance (W)	120 W	35 W	70.8% reduction
Charging current THD (%)	6.2%	2.1%	66.1% reduction
Stability under changes in step load	Marginal oscillations	No oscillations, Stable	Improved robustness
Converter efficiency (%)	95.0	96.5	+1.5
Voltage regulation error (%)	±4.8	±1.2	75% reduction
DC-link voltage settling time (ms)	180	65	63.9% faster
Output voltage overshoot (%)	8.5	2.1	75.3% reduction

3.3. Analysis of voltage gain and stability in resonant converters

The stability of the CLLLC resonant converter to EV charging at the battery voltages of 250 V, 350 V, and 450 V in a switching frequency range of 1 kHz-200 kHz was also evaluated using gain and phase margin studies, as shown in Figure 6. Figures 6(a) and 6(b) the open-loop system was not very stable in terms of gain margin available at 4-6 dB and a phase margin of 18°-22°. PI control gave the phase margin of 35°-40° and closed-loop gain margin of 12.4 dB; however, oscillations and phase error (±8°–10°) were noted in dynamic voltage swings. By contrast, the ANN-controlled converter was significantly more stable, with a gain margin of 18-20 dB and a phase margin of more than 62°, and a phase error range of ±2°–3°, compared to 30–35 ms with the PI controller, as shown in Figure 6(c) [22]-[24]. The ANN system was found to be stable in voltage gain and soft-switching behavior in all operating conditions, fully 96.5% more efficient than 94% when used with the PI-controlled converter. These findings prove that ANN control offers better stability, rapid transient response, and efficiency of dynamic EV charging. The operation of a resonant converter defines the EV charging power during 24 hours, as shown in Figure 6(d). The model operates over a 0 to 24-hour time range with a 0.5-hour time interval, and the converter generates 200-400 V at 20 V increments. The demand analysis represents the activity of charging the EV with the help of a cosine-based demand factor, which is the combination of peak time and the off-peak period. To gain a clearer insight into the optimal ways of charging an EV, this assessment examines voltage control within the CLLLC converter that dictates the amount of power to charge daily.

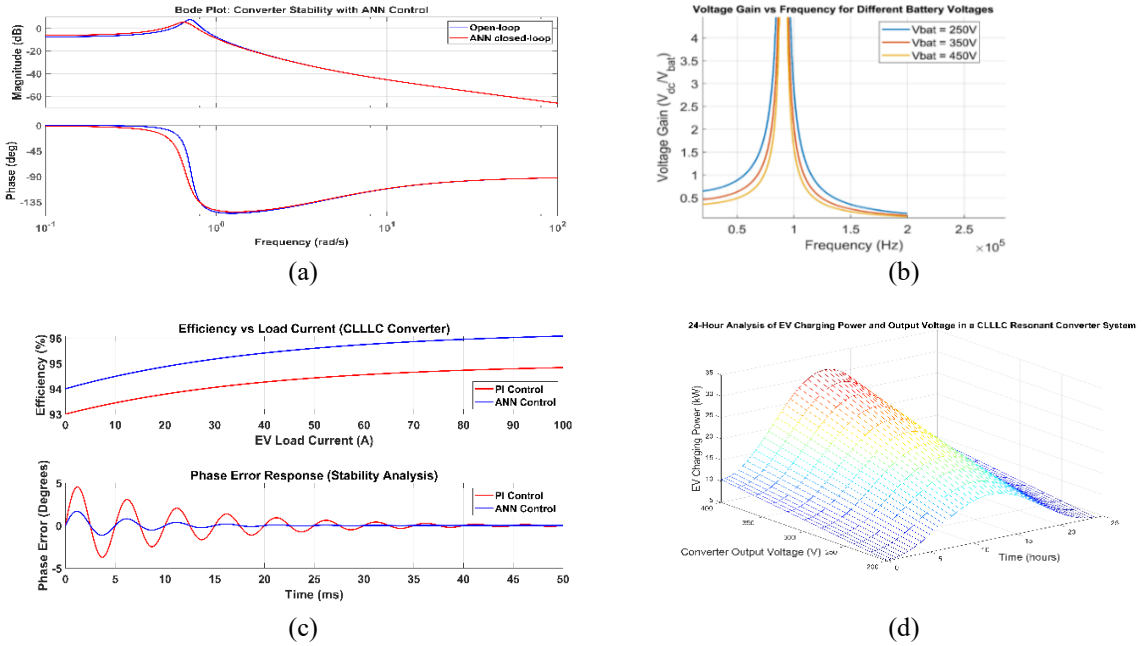

Figure 6. Converter quality and stability analysis; (a) Bode response, (b) voltage gain, (c) efficiency and phase error, and (d) EV charging power over 24 hours

4. EXPERIMENTAL IMPLEMENTATION

The hardware results of the solar EV charging system are shown in Figure 7. The entire hardware configuration, which includes a 30 V, 300 W photovoltaic panel, an MPPT-based DC–DC converter, and an isolated high-frequency resonant converter, is depicted in Figure 7(a). The primary-side high-frequency transformer voltage, which is measured at roughly 24–28 V and operates in the 20 kHz range, is shown in Figure 7(b), indicating soft-switching operation. The secondary-side transformer voltage, stepped down to roughly 15–16 V AC in accordance with the intended turns ratio, is shown in Figure 7(c). Lastly, Figure 7(d) validates steady and secure charging performance by displaying the regulated DC output voltage of 13.8–14.4 V delivered to the EV lithium-ion battery under BMS control [25].

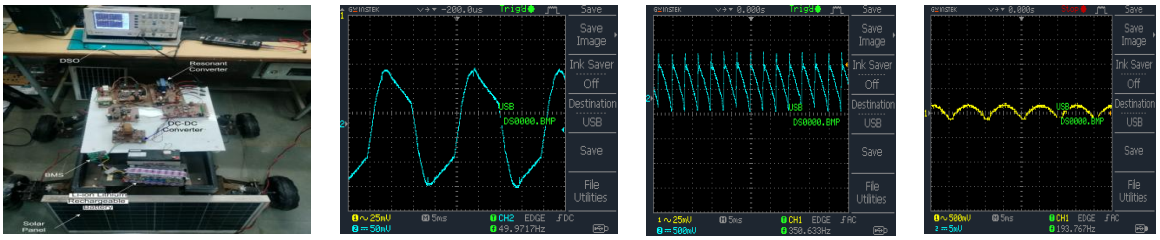

(a) (b) (c) (d)

Figure 7. Solar EV charger; (a) hardware setup, (b) primary side HF transformer voltage, (c) secondary side voltage, and (d) DC voltage to EV battery

5. CONCLUSION AND FUTURE WORK

The performance of the EV charger under dynamic conditions of battery load and solar fluctuation. The resonant converter controlled by the ANN-based and PI strategies exhibited more rapid convergence of the MPPT, increased tracking, and a more stable charging current than a more traditional controller. It also ensured a smooth SOC transition, which enhanced battery safety and energy efficiency. The PI controller for the resonant converter was limited in its real-time usage due to delayed response and oscillations when the load was changed abruptly. In the case of complex and high-performance EV charging systems, the ANN-based control is the most appropriate one, as it is capable of effectively adapting to the shifting load requirements and solar input. These results justify the feasibility of ANN-integrated resonant converters to be implemented in smart grid and renewable energy-based charging infrastructure. The further studies will be focused on the practical use of the proposed ANN-based solar EV charging system in practice, where the IoT-based real-time control of the PV output, battery state-of-charge, and charger health will be implemented. AI-based predictive maintenance will also be explored to enhance the reliability of the converters and batteries. The controller will also be extended to hybrid solar-grid charging designs to ensure that power sharing is smooth and power charging takes place even when the irradiance is low and under peak demand conditions.

REFERENCES

[1] M. A. Kamoona, J. Manuel Mauricio, A. L. Saleh, and L. Számel, "Advanced MPPT strategy for PV solar energy systems using ANN-GWO," in *2024 6th Global Power, Energy and Communication Conference (GPECOM)*, IEEE, Jun. 2024, pp. 439–444. doi: 10.1109/GPECOM61896.2024.10582686.

[2] S. Chayma and F. Aymen, "Comparative analysis of P&O and ANN MPPT algorithms in conventional and floating solar photovoltaic systems," in *2024 6th International Symposium on Advanced Electrical and Communication Technologies (ISAECT)*, IEEE, Dec. 2024, pp. 1–6. doi: 10.1109/ISAECT64333.2024.10799631.

[3] B. Latha, M. Mujahid Irfan, and B. Koti Reddy, "Enhanced wireless power transfer for electric vehicles: A 7.2 kW ANN-based MPPT approach with LCC-LCC compensation topology," *Energy Reports*, vol. 14, pp. 2157–2169, 2025, doi: 10.1016/j.egyr.2025.08.039.

[4] N. Kumari and M. Singh, "Controlling grid-connected PV array with P&O MPPT," in *2024 IEEE 4th International Conference on Sustainable Energy and Future Electric Transportation (SEFET)*, IEEE, Jul. 2024, pp. 1–6. doi: 10.1109/SEFET61574.2024.10718047.

[5] N. Deghfel, A. E. Badoud, A. A. Al-Ahmadi, M. Bajaj, I. Zaitsev, and S. S. M. Ghoneim, "Improving maximum power point tracking efficiency in solar photovoltaic systems using super-twisting algorithm and grey wolf optimizer," *IET Renewable Power Generation*, vol. 18, no. 15, pp. 3329–3354, Nov. 2024, doi: 10.1049/rpg2.13138.

[6] Z. Xiao, X. Li, and Y. Tang, "A lightweight artificial neural network start-up controller for CLLC resonant converters," *IEEE Transactions on Power Electronics*, vol. 39, no. 11, pp. 14775–14786, Nov. 2024, doi: 10.1109/TPEL.2024.3436847.

[7] M. A. A. Ashiq, L. J. S. Shanthi, G. Sivasankar, and C. Balasundar, "Bridgeless canonical and buck-boost converter combined artificial neural network controlled efficient battery charger for electric vehicles," *Electric Power Systems Research*, vol. 248, p. 111944, Nov. 2025, doi: 10.1016/j.epsr.2025.111944.

[8] S. Chauhan and B. Singh, "Grid-interfaced solar PV powered electric vehicle battery system with novel adaptive digital control algorithm," *IET Power Electronics*, vol. 12, no. 13, pp. 3470–3478, Nov. 2019, doi: 10.1049/iet-pel.2019.0025.
[9] R. Manoharan and R. S. Wahab, "Model predictive controller-based convolutional neural network controller for optimal frequency tracking of resonant converter-based EV charger," *Results in Engineering*, vol. 24, p. 103658, Dec. 2024, doi: 10.1016/j.rineng.2024.103658.
[10] M. K. N, S. Y, P. Whitin, and J. Y, "Enhanced regulation and optimization techniques for isolated fourth-order l3c resonant converters in solar pv to battery pack conversions," *Journal of Energy Storage*, vol. 116, 2025, doi: 10.1016/j.est.2025.115693.
[11] P. Pal, R. K. Behera, and U. R. Muduli, "Feedforward repetitive approach to disturbance rejection in DAB converters for EV charging," *IEEE Transactions on Industrial Electronics*, vol. 72, no. 8, pp. 7861–7873, Aug. 2025, doi: 10.1109/TIE.2024.3519565.
[12] A. B. Rehiara, E. K. Bawan, A. D. Palintin, B. R. Wihyawari, F. Y. Setiawan Paisey, and Y. R. Pasalli, "Probabilistic load flow based voltage stability assessment of solar power integration into power grids," *Bulletin of Electrical Engineering and Informatics (BEEI)*, vol. 13, no. 4, pp. 2231–2241, Aug. 2024, doi: 10.11591/eei.v13i4.5651.
[13] N. The Vinh and N. Van Dung, "Flexible converter for electric vehicle charging station using renewable energy efficiently," *International Journal of Technology*, vol. 16, no. 5, pp. 1800–1815, Sep. 2025, doi: 10.14716/ijtech.v16i5.7701.
[14] S. Sarath and K. Vijayakumar, "High-gain MSHS converter with TCH-DAG controlling model for smart PV-EV charging systems," *Journal of Energy Storage*, vol. 134, p. 118318, Oct. 2025, doi: 10.1016/j.est.2025.118318.
[15] V. Powar and R. Singh, "End-to-end direct-current-based extreme fast electric vehicle charging infrastructure using lithium-ion battery storage," *Batteries*, vol. 9, no. 3, p. 169, Mar. 2023, doi: 10.3390/batteries9030169.
[16] A. Kusmantoro and I. Farikhah, "Power management on DC microgrid with new DC coupling based on fuzzy logic," *Indonesian Journal of Electrical Engineering and Computer Science (IJEECS)*, vol. 32, no. 2, pp. 620–631, Nov. 2023, doi: 10.11591/ijeecs.v32.i2.pp620-631.
[17] G. A. Mudiyanselage, K. Kozielski, and A. Emadi, "Optimal LLC converter design with topology morphing control for wide voltage range battery charging applications," *IEEE Open Journal of Power Electronics*, vol. 5, pp. 1209–1226, 2024, doi: 10.1109/OJPEL.2024.3444775.
[18] U. Avulamanda, M. K. Banda, S. Madichetty, and S. Mishra, "Comparative analysis of resonant converters for EV charging applications," in *2025 13th International Electrical Engineering Congress (iEECON)*, IEEE, Mar. 2025, pp. 1–6. doi: 10.1109/iEECON64081.2025.10987833.
[19] A. F. Bendary, *et al.*, "Proposed ANFIS based approach for fault tracking, detection, clearing and rearrangement for photovoltaic system," *Sensors*, 2021, vol. 21, 2269, doi: 10.3390/s21072269.
[20] Y. Hakam, H. Ahessab, A. Gaga, M. Tabaa, and B. El Hadadi, "Design and simulation of a 5 KW solar-powered hybrid electric vehicle charging station with a ANN–Kalman filter MPPT and MPC-based inverter control for reduced THD," *Scientific African*, vol. 27, 2025, doi: 10.1016/j.sciaf.2025.e02563.
[21] M. Umair, N. M. Hidayat, A. Sukri Ahmad, N. H. Nik Ali, M. I. M. Mawardi, and E. Abdullah, "A renewable approach to electric vehicle charging through solar energy storage," *PLOS ONE*, vol. 19, no. 2, p. e0297376, Feb. 2024, doi: 10.1371/journal.pone.0297376.
[22] P. Muthukumar, M. Venkateshkumar, and C. S. Chin, "A comparative study of cutting-edge bi-directional power converters and intelligent control methodologies for advanced electric mobility," *IEEE Access*, vol. 12, pp. 28710–28752, 2024, doi: 10.1109/ACCESS.2024.3360267.
[23] P. R. Shankar and G. Arunkumar, "A novel approach to modeling and experimenting a solar-fed H6 configuration for battery swapping stations in rural and commercial areas using a dual phase CLLC DC–DC resonant converter," *Journal of Energy Storage*, vol. 89, p. 111609, Jun. 2024, doi: 10.1016/j.est.2024.111609.
[24] P. Y. Reddy and L. C. Saikia, "Optimized intelligent power quality control strategy for hybrid alternating current-direct current microgrid with electric vehicle charging," *Computers and Electrical Engineering*, vol. 124, p. 110397, May 2025, doi: 10.1016/j.compeleceng.2025.110397.
[25] A. K. M. A. Habib and M. K. Hasan, "Lithium-ion battery state-of-charge balancing circuit using single resonant converter for electric vehicle applications," *Journal of Energy Storage*, vol. 61, p. 106727, May 2023, doi: 10.1016/j.est.2023.106727.

BIOGRAPHIES OF AUTHORS

Rajeshkumar Damodharan was granted a B.E. in Electrical Engineering in 2009, an M.E. in Power Systems in 2013, and Ph.D. scholar at Vels Institute of Science, Technology and Advanced Studies (VISTAS), Chennai, India. He is an Assistant Professor in the Department of Electrical Engineering at Finolex Academy of Management and Technology (FAMT), Ratnagiri, India. He also has an industrial background in electrical engineering. Power systems, electrical machinery, switchgear and protection, electrical drives and control, and fundamental electrical engineering are among his areas of interest in both teaching and research. He can be contacted at email: d.rajeshkumar.reddy@gmail.com.

Dr. Pradeep Kumar S has 12 years and 4 months of academic experience as the Head of the Department and Associate Professor in the Department of Electrical and Electronics Engineering at Vels Institute of Science, Technology and Advanced Studies (VISTAS), Chennai, India. He has a Ph.D. in Electrical Engineering and an M.E. in Power Electronics and Drives. Power electronics, drives, artificial intelligence, and renewable energy systems are among his areas of interest in study. He has contributed significantly to the current study's conceptualization and technical validation.